ACS APPLIED ELECTRONIC MATERIALS

pubs.acs.org/acsaelm Article

Room-Temperature Sub-ppm Detection and Machine Learning-Based High-Accuracy Selective Analysis of Ammonia Gas Using Silicon Vertical Microwire Arrays

Quang Trung Le, Ali Sehpar Shikoh, Kumin Kang, Jeongho Lee, and Jaekyun Kim*

Cite This: ACS Appl. Electron. Mater. 2023, 5, 357−366 Read Online

ACCESS | Metrics & More | Article Recommendations | Supporting Information

ABSTRACT: The potential applications of silicon microwire materials in monitoring gases have not been fully exploited. Uniform silicon vertical microwire arrays (Si VMWA) are fabricated using a metal-assisted chemical etching process after optimizing the conditions. The characteristics and responses of Si VMWA-based sensors with different diameters to ammonia gas (NH_3) are investigated in both air and nitrogen environments. The sensing mechanism of the sensor to NH_3 is discussed to clarify the response in different environments. The sensor exhibits a linear response to a wide range of NH_3 concentrations (4%@2 ppm−122%@500 ppm) at room temperature and even shows a distinct response at 200 ppb of NH_3. In addition, it demonstrates great repeatability/reversibility and moderate selectivity to ammonia gas against other gases (nitrogen dioxide, toluene, and isobutane). Furthermore, machine learning-based principal component analysis and random forest algorithms enable us to discriminate NH_3 from other possible interfering gases and predict gas concentration with an accuracy of over 95%. Thus, our approach using the Si VMWA-based sensor with machine learning-based data analysis represents a significant step toward the environmental sensing of specific chemical analytes in the household and industries.

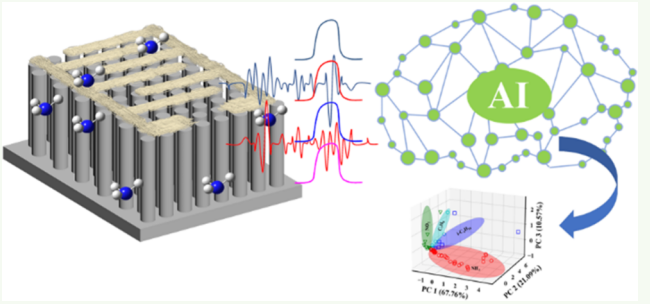

KEYWORDS: *silicon microwires, MaCE, ammonia, gas sensor, silver nanowire, machine learning*

1. INTRODUCTION

Along with industrial development and modern life demand, the necessity of monitoring exhausted hazardous gases, such as hydrogen sulfide, carbon oxides, nitrogen oxides, ammonia, chlorine, and volatile organic compounds, has rapidly increased in recent years due to their catastrophic impact on human health, the ecosystem, and the environment. In particular, ammonia (NH_3) gas is classified as a highly hazardous substance as it is very harmful to the human body involving the skin, eyes, lungs, and can even lead to death. In addition, monitoring the presence of NH_3 in exhaling is a critical biomarker for diagnosing diseases, such as chronic kidney diseases and peptic ulcers.[1,2] Thus, it is imperative to develop reliable, susceptible, and selective sensors to detect NH_3 at room temperature with a facile and low-cost fabrication.

Various methods and materials have been studied to monitor NH_3 gas, including electrochemical, polymer, surface acoustic wave, metal oxide (MO)-based sensors, and others.[3−8] Among them, the MO-based sensors (TiO_2, WO_3, ZnO/SnO_2, NiO/ZnO...) have drawn significant interest due to their facile, low cost, and flexible fabrication approaches.[9] Nevertheless, the poor selectivity and the high working temperature requirement (200−500 °C) are critical drawbacks.[10] Recently, two-dimensional (2D) materials, such as graphene, $MoSe_2$, WS_2, MoS_2, and MXene, have been studied for applications in sensing devices due to their large specific surface areas.[11] Theoretical studies indicated the potential of MXene in monitoring NH_3 gas due to the strong interaction between Ti_2C_3 and NH_3.[12] Graphene and hybrid structures exhibited great ability in NH_3 gas sensing at room temperature.[13,14] The modification of 2D materials with noble nanoparticles is a common method to improve gas sensing performance.[15] However, employing noble nanoparticles is an expensive approach. In addition, the recovery and selectivity of these materials to gases are obstacles in practical applications. Although the 2D structure of MO nanosheets, such as ZnO or NiO synthesized through the hydrothermal reaction, showed remarkable selectivity to gases,[9] the high working temperature requirement prohibits practical applications at room temperature.

As advanced silicon technology accelerated, silicon became one of the most prominent materials for fabricating low-cost

Received: October 11, 2022
Accepted: January 5, 2023
Published: January 12, 2023

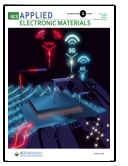

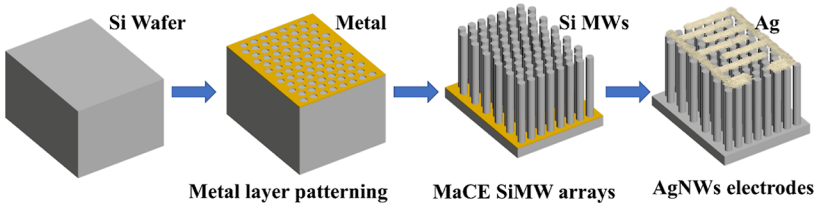

Figure 1. Schematic diagram of the Si VMWA-based ammonia gas sensor fabrication.

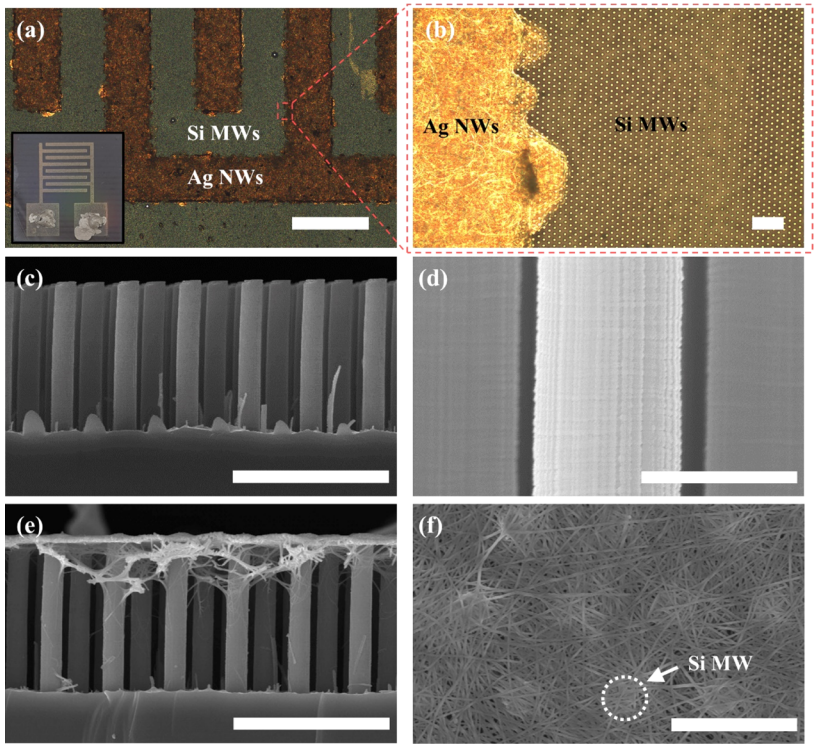

Figure 2. (a,b) Microscopic images of post-sprayed AgNW IDEs structure on SiMW (scale bar of 500 and 10 μm, respectively). Inset in (a) shows the practical image of a typical device. (c) Cross-sectional scanning electron microscopy (SEM) image of SiMW with the desired length of approximately 10 μm (scale bar of 10 μm); (d) rough surface of post-MaCE SiMW (scale bar of 2 μm); (e) sprayed AgNW staying on top of SiMW as the internetwork layer (scale bar of 10 μm); and (f) top view SEM image of AgNW layer (scale bar of 5 μm).

electronic devices, especially in chemical sensing applications. The ability of silicon nanowire (SiNW) material in NH_3 gas sensing at room temperature was introduced,[16] followed by studies functionalizing the surface of SiNW with MOs, noble metals, polymers, and heterojunction materials[17−20] to enhance the NH_3 gas sensing performance. However, the fabrication of SiNW through the methods such as using polystyrene sphere lithography, nanoimprinting, e-beam lithography, deep reactive ion etching, and vapor−liquid−solid growth involves complicated and expensive multi-step processes.[21−23] In contrast to SiNW, the silicon microwire (SiMW) fabrication through the metal-assisted chemical etching (MaCE) method is relatively facile and low cost. SiMW was evaluated as a potential candidate for a next-generation solar energy conversion materials.[21] It has been employed in various energy applications, such as hydrogen generation and lithium-ion batteries.[24−26] Nevertheless, the potential application of SiMW materials in monitoring gases has not been fully exploited. Although microelectromechanical systems structure-based SiMWs exhibited VOCs' gas sensing potential of silicon materials at the microsize, the structure with a size of over 100 μm is not sensitive to gases.[27] Modifying the surface of SiMWs with other MOs, such as In_2O_3 or ZnO, can improve the sensing performance.[28,29] However, the high working temperature and narrow detection range are drawbacks of these structures. In order to enhance the selectivity of silicon materials, SiNWs were modified with noble nanoparticles, 2D materials, such as MoS_2, organic semiconductors, and carbon material, or functionalized the surface of SiNWs by chemical treatment.[30] Besides that, an array of chemical-sensitive field effect transistor platforms were fabricated based on silicon, Pd−Au, Ni−Pd, and Ni, exhibiting a remarkable selectivity to H_2S, H_2, and NO_2.[31] However, the use of the array of sensors not only consumes more energy but also requires more complicated fabrication processes than a single sensor. Meanwhile, gas adsorption and desorption processes on the materials are strongly related to the chemical and physical properties of gases.[32,33] Hence, extracting the relationship between the sensor response and the adsorption/desorption of the analyte is valuable information to enhance the discrimination of gases through machine learning algorithms, consequently improving the selectivity feature of the single sensor platform.

https://doi.org/10.1021/acsaelm.2c01383
ACS Appl. Electron. Mater. 2023, 5, 357−366

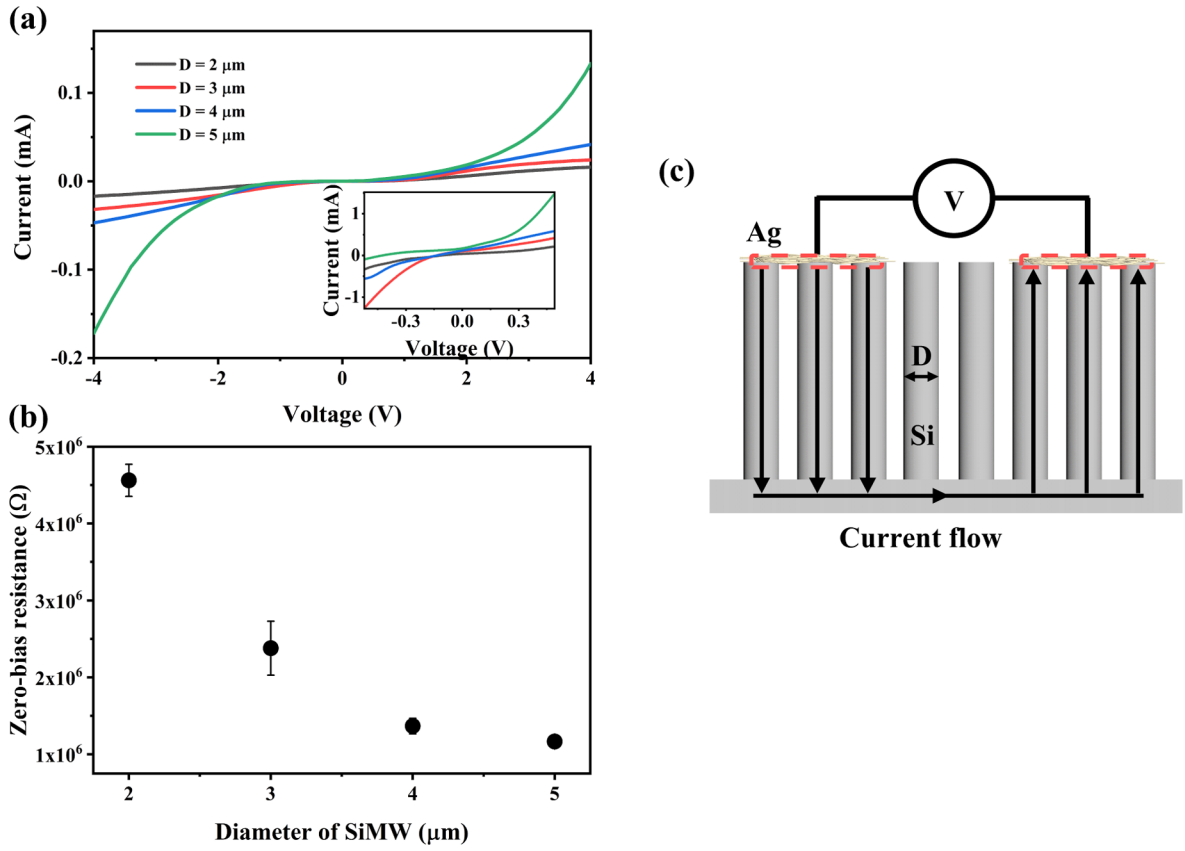

Figure 3. (a) Current−voltage characteristics with various diameters of Si VMWA and (b) extracted zero-bias resistance with SiMW diameter variations. (c) Current path of vertical Si VMWA (diameter D) with AgNW network contact electrodes.

In this study, a convenient process to fabricate a low-cost high-performance NH_3 gas sensor has been introduced. Conventional photolithography technology was used to pattern the microstructure onto silicon substrates. Subsequently, the silicon vertical microwire arrays (Si VMWAs) were fabricated via the MaCE process after optimizing the reaction conditions. The as-fabricated Si VMWA was introduced with silver nanowires (AgNWs) as the interdigitated electrode (IDE) and was then employed as an NH_3 gas sensor. Machine learning-based random forest (RF) classification algorithm and principal component analysis (PCA) methods were utilized to analyze the extracted data set, enhancing the gas discrimination and concentration prediction of the sensor.

2. EXPERIMENTAL SECTION

2.1. Si VMWA-Based Sensor Fabrication. The Si VMWA-based sensor fabrication scheme is depicted in Figure 1. Si VMWA substrates with different diameters (2−5 μm) were fabricated according to previous reports[23] with modifications described in section S1.3 (Supporting Information). An IDE structure shadow mask (Figure S1a) with 4 pairs of fingers (a length of 4400 μm, width of 300 μm, and gap of 300 μm) was prepared and placed on the top of the Si VMWA substrate. The AgNW IDE electrode was fabricated by spray-coating for 5 min with a nozzle sprayer at a fixed distance between the sprayer and substrate of 30 cm. A 60 °C hot plate was utilized during the spray-coating to accelerate the evaporation of the isopropyl alcohol solvent of the AgNW suspension. Finally, small silver paste drops were introduced at the head of electrode pads as the contact areas (Figure 2a inset) and dried under ambient conditions.

2.2. Resistance Measurement for Gas Sensing. The resistance changes of the Si VMWA with the introduction of NH_3 gas were investigated at room temperature (25 °C). Analyte gas samples were generated from standard gas cylinders with a gas concentration of 1000 ppm mixed with dried synthetic air (oxygen 21% and nitrogen 79%) as the balance gas.[17] The desired concentration of NH_3 gas was obtained by controlling a volume of 1000 ppm NH_3 gas and synthetic air exposed as the following equation

$$C_{NH_3\text{-target}} = C_{NH_3\text{-1000ppm}} \times V_{NH_3\text{-1000ppm}}/(V_{air} + V_{NH_3\text{-1000ppm}})$$

where $C_{NH_3\text{-target}}$ and $C_{NH_3\text{-1000ppm}}$ are the target and source concentrations (1000 ppm) of NH_3 gas, respectively. $V_{NH_3\text{-1000ppm}}$ and V_{air} are the volumes of source NH_3 gas and synthetic air, respectively. Humidity was introduced using distilled water through a bubbler system, as depicted in Figure S1. A commercial sensor (Bosch BME680) was employed to determine the relative humidity (RH). The analyte concentration and RH were adjusted through a computer-connected mass flow controller system with a total flow of 1000 sccm. The applied DC bias voltage was fixed at 4 V in all experiments. The resistance response was recorded via a Keithley 2636B model. At the beginning of the sensing measurement, synthetic air was introduced for 30 min to achieve stable conditions. The sensor response was defined as the following equation[34]

$$R\ (\%) = \frac{\Delta R}{R_{air}} = \frac{R_{gas} - R_{air}}{R_{air}} \times 100\%$$

where R_{gas} and R_{air} are resistances recorded with and without analyte gases, respectively. Exposure times with and without analyte gases were 300 and 500 s, respectively. The response time is the span required to reach 90% of the highest response after introducing the analyte gas. The recovery rate is expressed as recovery rate (%) $= (R_g - R_r)/(R_g - R_0)$,[35] where R_0 and R_g are the resistance values in synthetic air and after 300 s exposure to NH_3

https://doi.org/10.1021/acsaelm.2c01383
ACS Appl. Electron. Mater. 2023, 5, 357−366

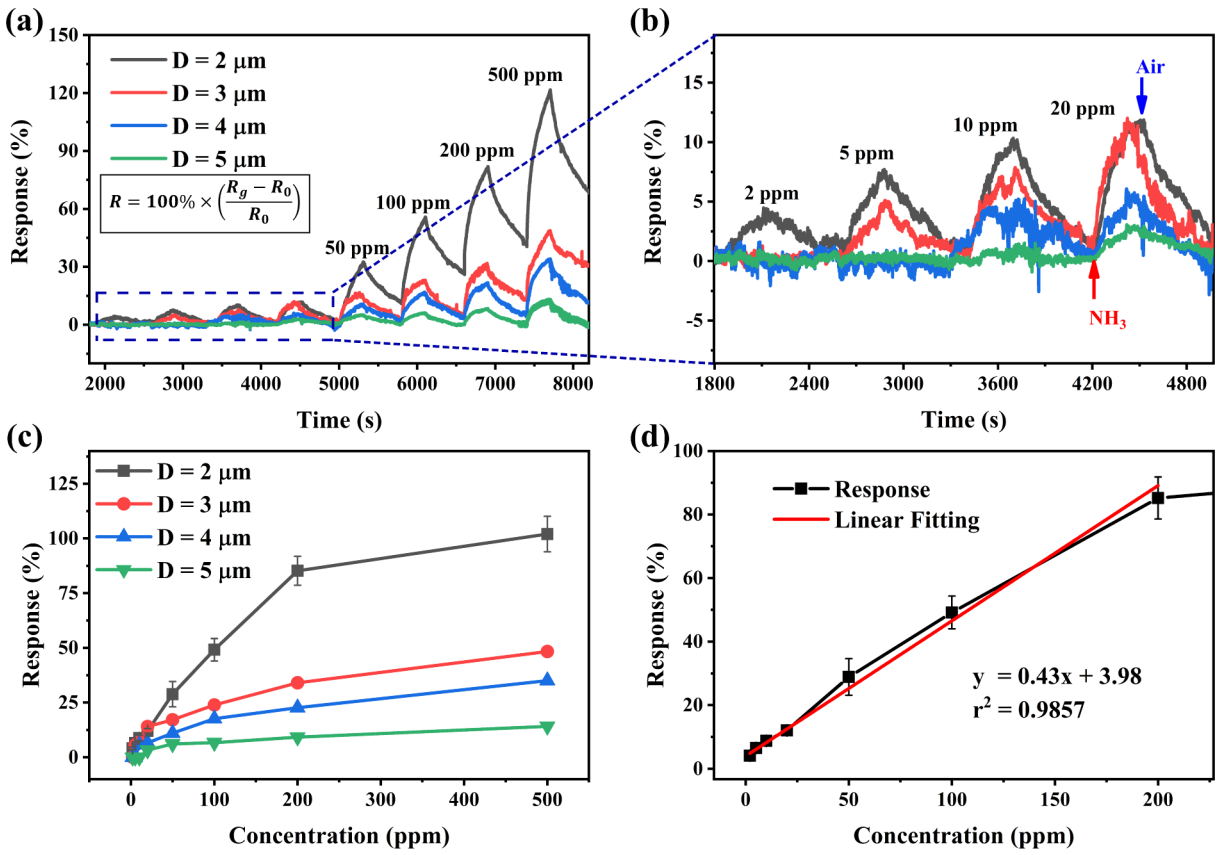

Figure 4. (a−c) Sensing performance of Si VMWA at different diameters (2, 3, 4, and 5 μm) to ammonia gas at various concentrations with (d) linear response in the concentration range of 2−200 ppm. (RH 0%).

gas, respectively. R_r is the recovered resistance value after exposure to synthetic air for 500 s.

2.3. Machine Learning Technique. PCAs and discrimination models based on the RF machine learning algorithms, including classifiers and regressors with 1000 trees in the forest, were employed to perform the gas discrimination and NH_3 gas concentration prediction. Gas types, concentrations, responses, resistances, and slopes[33] of the Si VMWA-based sensor response curve to gases at different concentrations were extracted as the input data for machine learning. The prediction accuracy of the algorithms was investigated based on the divided training and testing data sets with a ratio of 60:40. The open source scikit-learn libraries[36] were used on Python v3.8.12[37] with a PyCharm-integrated development environment.

3. RESULTS AND DISCUSSION

3.1. Si VMWA-Based Sensor Fabrication and Electrical Characterization. Figure 2 illustrates the optical microscopy and SEM images of the sensing device. The Si VMWA with a length of approximately 10 μm was fabricated by the MaCE method (discussed in section S2, Supporting Information). AgNW was spray-coated to fabricate the IDE electrode on Si VMWA substrates. Compared with conventional electrode structures,[18,38] the number of SiMW involved in the sensing increase with the IDE structure. The intertwined AgNW layer is stable on the top of the Si VMWA as the mesh structure and electrically connects the tips of SiMW (Figure 2e,f). This mesh structure allows the gas molecules to penetrate freely through it and interact with the sensing material. Because the gap between adjacent SiMW is approximately 2 μm, AgNW (about 25 μm in length) is a suitable material to connect SiMW tips, avoiding AgNW dropping to the bottom. AgNW, a solution-processable and low-cost material with good conductivity and flexibility, was employed to fabricate electrodes in lighting devices[39] and solar cells.[40] Markedly, the AgNW material was also reported as the NH_3 gas-sensing material, but it can only sense at a high concentration (3%).[41]

Figure 3a shows the $I-V$ characteristic curves of the Si VMWA devices with the same wire length of 10 μm and various wire diameters (2, 3, 4, and 5 μm, depicted as D_2, D_3, D_4, and D_5 samples, respectively). With the same length and gap between adjacent SiMW, the increase in SiMW diameter results in the resistance decrease, accordingly, and conductivity increase of the Si VMWA device. Zero-bias resistance ($R = [dV/dI]/V = 0$)[42] decreases with the increase in the diameter of SiMW (Figure 3b). Due to the smaller diameter of SiMW, the contact area with the AgNW network is narrower (Figure 3c), consequently resulting in higher contact resistance. At 4 V, the D_5 and D_2 samples exhibit the highest and the lowest conductance, respectively. Figure 3c also depicts the current path of our device configuration. The current path performs along the length of SiMWs and substrates between the electrodes. During the gas-sensing measurement, on account of our IDE configuration, myriad active sites can be involved to enhance gas-sensing performance.

3.2. Highly Effective Performance in NH_3 Gas Sensing of Si VMWA Device. AgNWs in planar structures and IDE structures were prepared on bare silicon substrates. Subsequently, NH_3 gas with a concentration of 500 ppm was exposed to observe the response. As shown in Figure S6, these two sensing structures obtain negligible responses to NH_3 500 ppm. The result proves that the sensing performance of Si VMWA devices is produced from silicon materials instead of

https://doi.org/10.1021/acsaelm.2c01383
ACS Appl. Electron. Mater. 2023, 5, 357−366

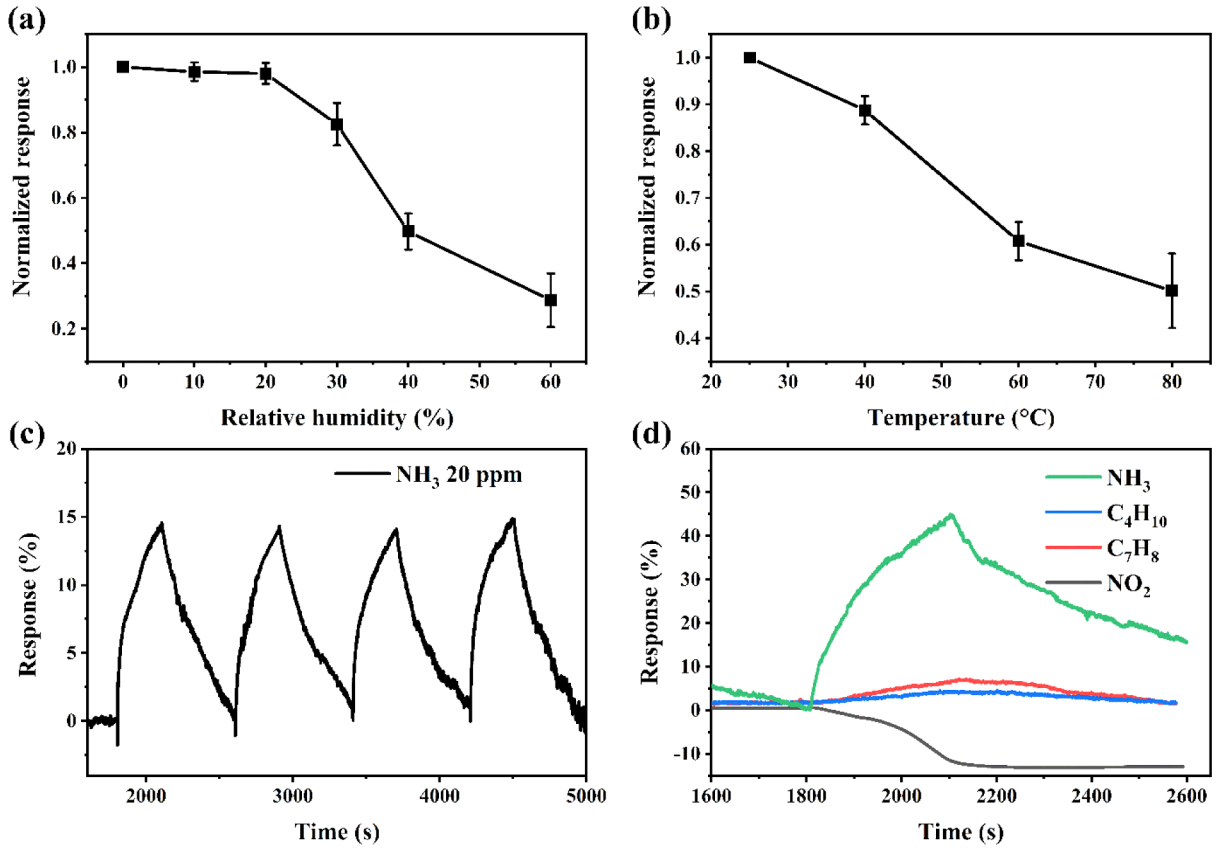

Figure 5. Normalized response of Si VMWA to 100 ppm of ammonia gas (a) at different RH and (b) at different temperatures (RH 0%); (c) cyclic response curve of Si VMWA to 20 ppm of ammonia gas at room temperature (RH 0%); and (d) selective response of Si VMWA to 100 ppm concentration of different gases at room temperature (RH 0%).

AgNW. Figure 4a,b depicts the variation of sensing performance of samples with different microwire diameters to NH_3 gas at a wide range of gas concentrations, from 2 to 500 ppm. The D_2 sample with the smallest diameter exhibits the highest response to the NH_3 gas, approximately 4−122% at 2−500 ppm of NH_3 gas, respectively. The response gradually decreases with the increase in the SiMW diameter. The sample with a smaller diameter provides a more significant SiMW density and a larger surface area involved in the NH_3 adsorption. As shown in Figure 2d, the rough surface of as-fabricated SiMW can provide a large area for gas adsorption onto the SiMW. Figure 4c illustrates the response changes as a function of NH_3 gas concentration from 2 to 500 ppm of Si VMWA devices with different diameters. At a NH_3 gas concentration higher than 200 ppm, the response of the D_2 sample tends to be saturated. The D_5 sample is saturated at a lower gas concentration (50 ppm). This behavior can be attributed to SiMW channels being sensitive to gas adsorption but having a restricted active area on the sidewall. Figure 4d depicts the corresponding standard curve of the response of the D_2 sample to NH_3 gas in a concentration range of 2−200 ppm. Based on the response of the device to the known concentration of NH_3 gas, the linear regression mathematical equation can be expressed as $y = ax + b$, where y, a, x, and b are the response, slope, gas concentrations, and y-axis intercept values, respectively. The correlation coefficient (r^2) of the calibration curve is 0.9857. The limits of detection (LOD) can be determined via the response standard deviation (Sy) and the calibration curve slope (a) as LOD = 3.3 × (Sy/a) = 180 ppb.[43] NH_3 gas flow with a concentration of 200 ppb was introduced into the sensing chamber to confirm the theoretical LOD value. Figure S7 depicts the distinct response of the sensor to 200 ppb of NH_3 gas.

In addition, the response of the Si VMWA sensor to NH_3 gas was measured in a nitrogen gas environment by recording the conductance change.[44,45] As depicted in Figure S8, the Si VMWA sensor response is extremely sensitive to NH_3 gas in a nitrogen environment. The sensor exhibits a response of 40−7800% to NH_3 gas in a gas concentration range of 2−500 ppm, with a linear response in the range of 2−200 ppm. Results measured in nitrogen gas show the opposite behavior to those in synthetic air. In the nitrogen environment, the conductance increases with exposure to NH_3, which means the resistance decreases. The different response behavior mechanisms will be discussed in Section 3.3.

The effect of temperature (25 to 80 °C) and humidity (0 to 60%) on the response curves of the Si VMWA sensor were investigated, as they crucially influence sensors in practical applications. As can be seen in Figure 5a, humidity has a strong effect on the operating performance of the Si VMWA sensor. With the increase in RH from 0 to 30%, the response of the device to ammonia gas slightly decreases. A considerable decrease in the response value is observed at a humidity of over 30%. The drop in sensing response can be attributed to the fact that water molecules are adsorbed, cover the surface of silicon materials, and occupy the adsorption site. Therefore, the adsorption sites on the silicon surface decrease. Consequently, the number of adsorbed ammonia molecules decreases, leading to a lower response.[46,47] As illustrated in Figure 5b, the reduction of sensing responses with the temperature increase

https://doi.org/10.1021/acsaelm.2c01383
ACS Appl. Electron. Mater. 2023, 5, 357−366

was observed as the adsorbed gas decreased with the temperature rise. Hence, the sensing performance degrades. The operating temperature typically affects the gas-sensing performance of semiconductor materials due to the influences on semiconductor material characteristics. Besides that, the temperature directly affects the adsorption and desorption processes of gas on the material surface. However, the influence of humidity and temperature on gas sensing results can be subtracted using an additional sensor or machine learning technique.[48,49]

Figure 5c indicates the response of the sensing device to 20 ppm NH_3 gas. The result exhibits a good reproducibility of the device during cyclic gas exposure. The selectivity to NH3 gas against other gases of the sensor was also investigated, including nitrogen dioxide (NO_2), isobutane (i-C_4H_{10}), and toluene (C_7H_8). Figure 5d shows the selectivity of the Si VMWA-based sensor, where 100 ppm of different gases was separately introduced into the chamber. The Si VMWA-based sensor exhibits a much higher response to the NH_3 gas than the others. It can be attributed to the strong interaction between the reducing NH_3 gas and the exposed surface of SiMW (Si−OH). The highest response upon the exposure of NH_3 gas promises that the selective detection of NH_3 gas from a mixture can be achieved by Si VMWA-based gas sensors.

At room temperature, the response time (t_{res}) is approximately 200 s and decreases with the gas concentration increase (Figure S9b). Due to the strong chemisorption of silicon material to NH_3 molecules,[50] the recovery of the Si VMWA-based sensor is impeded (Figure S9c). The recovery rate decreases with the increase in the gas concentration. At a concentration below 20 ppm, the sensor can recover about 95−98%. However, the sensor can recover about 65−70% of the initial state at higher concentrations. At low concentrations, ammonia molecules interact with oxygen molecules adsorbed on the surface of the silicon to produce nitrogen, water molecules, and electrons, which can be quickly released with exposure to synthetic air to recover the initial state. However, at higher concentrations, a large number of ammonia molecules can directly adsorb onto the surface of the silicon material due to high electronegativity and inhibit the release of ammonia gas from the surface due to the chemisorption of ammonia gas onto the silicon material.[50] Therefore, a longer time is required to release adsorbed ammonia molecules and recover the initial state. Besides that, edge sides and defects, which have high adsorption energy, formed on the surface of SiMWs during the fabrication are the positions where gas molecules are easily and mainly adsorbed, which slows down the recovery of the sensor. However, the recovery of the sensing device can be accelerated by applying thermal treatment after sensing. The results suggest that the Si VMWA device can operate at room temperature with an excellent sensing performance without additional heat energy, which requires a high-power consumption and limits the application in portable electronics. Therefore, in terms of sensing performance, the application of Si VMWA is comparable with other materials (Table 1).

3.3. Ammonia Gas Sensing Mechanism of Si VMWA Sensor. The sensing mechanisms of the Si VMWA sensor for ammonia gas in the air and nitrogen gas are illustrated in Figures S10 and S11, respectively. The AgNW mesh IDE configuration allows the free penetration of NH_3 gas to the SiMW surface. As can be seen in Figure 4a, the sensing behavior of our Si VMWA sensor is in accordance with other

Table 1. Summary of Various Ammonia Gas Sensing Materials[a]

materials	LOD	concentration (ppm)	response	temperature
SiNWs@Te[51]	196 ppb	100	~90%	RT
SiNWs@Ppy[19]	130 ppb	10	~10.1 (~910%)	RT
SiO_2@CeO_2[52]	500 ppb	80	3244%	RT
ZnO@Pd[53]	30 ppm	30	~12%	200 °C
CS[6]	10 ppm	50	50%	80 °C
ZnO@CNT[14]	200 ppb	100	6.4 (~540%)	RT
CNT[54]	100 ppb	10	5%	RT
Ti_3C_2 MXene[55]	10 ppm	100	2%	RT
graphene[13]	20 ppm	160	~8%	RT
PQT-12[56]	404 ppb	80	56.4%	RT
SiMW—this work	200 ppb	100	50%	RT

[a]RT: room temperature.

conventional p-type semiconductors, which have a resistance increase upon ammonia gas introduction. The oxygen molecule (O_2) is an essential component in studying the gas sensing mechanism. As illustrated in Figure S10, in the air environment, electrons transfer from the silicon material to O_2 due to the high electron affinity of the oxygen atoms, after O_2 from the air was adsorbed at the silicon surface, resulting in the formation of the chemisorbed oxygen species such as O^-, O^{2-}, and O_2^- on the silicon surface, which captures electrons of silicon. Therefore, a hole accumulation layer (HAL) playing the role of the carrier conduction channel is formed at the subsurface of silicon.[18] Upon exposure to ammonia gas, the adsorbed oxygen species react with the ammonia molecules and release captured electrons back to silicon as the following redox reactions[57−60]

$$2NH_3 + 3O^- \rightarrow N_2 + 3H_2O + 3e^- \quad (1)$$

$$4NH_3 + 3O_2^- \rightarrow 2N_2 + 6H_2O + 3e^- \quad (2)$$

$$2NH_3 + 3O^{2-} \rightarrow N_2 + 3H_2O + 6e^- \quad (3)$$

It should be noted that the temperature strongly affects the adsorption of oxygen molecules. O_2^- is commonly chemisorbed at low temperatures, while O^- and O^{2-} are chemisorbed at high temperatures.[57,58] Therefore, the primary redox reaction at room temperature is reaction 2, in which O_2^- reacts with NH_3 to release electrons. Electrons are released back to silicon through redox reactions resulting in electron−hole recombination. The number of holes, the majority carrier in p-type semiconductors, decreases. Consequently, the thickness of the HAL conducting channel decreases, and the resistance offered by Si VMWA decreases. With the increase of NH_3 gas concentration, more trapped electrons will be released. Thus, the conductance increases with the increase of gas concentration exposure.

As can be seen in Figure S8, in the nitrogen gas environment, the conductance of Si VMWA increases with exposure to ammonia gas, exhibiting a contrasting behavior to that in the air environment. The sensing mechanism of Si VMWA with ammonia gas in the nitrogen gas environment is illustrated in Figure S11. At room temperature, NH_3 molecules adsorb onto the silicon surface to form Si−NH_2 and Si−NH surface bonding species by capping the dangling bonds of Si═

https://doi.org/10.1021/acsaelm.2c01383
ACS Appl. Electron. Mater. 2023, 5, 357−366

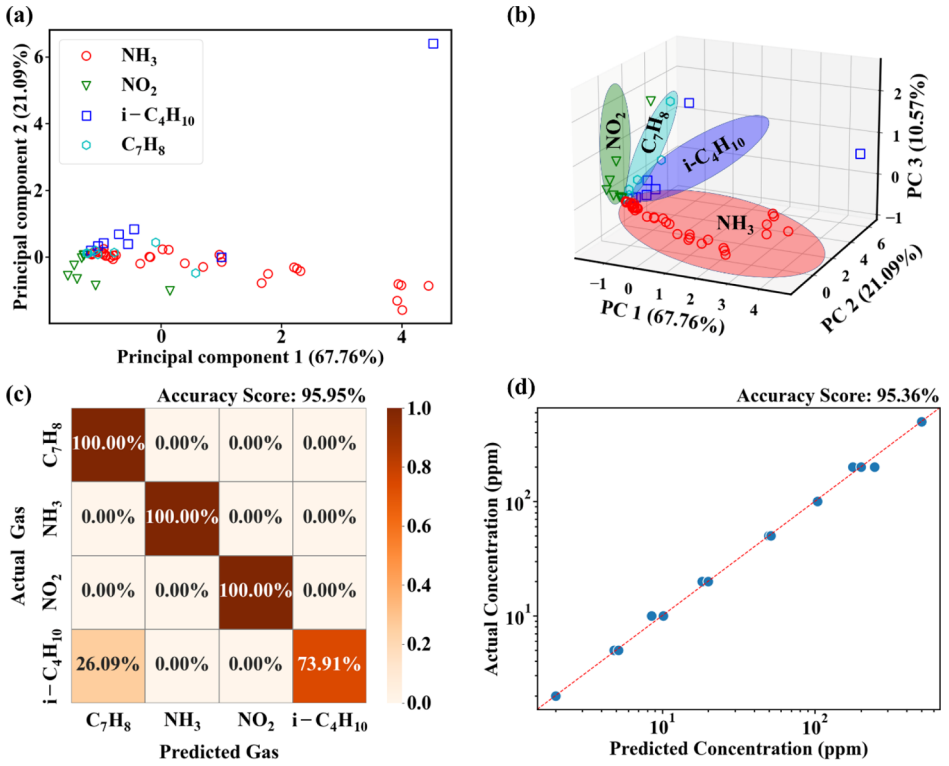

Figure 6. (a) 2D and (b) 3D PCA plots for the tested gases. (c) Normalized confusion matrix for the RF classifier and (d) predicted concentrations versus the actual concentrations for tested ammonia gas (log scale).

Si and Si−H,[61−64] which was supposed to be of importance in binding atomic nitrogen to silicon.[65] As a highly electron-donating agent, NH_3 molecules can strongly interact with −H and −OH terminals on the SiMW surface and transfer charges to the SiMW, leading to a rise in charge density in the channel.[66] Consequently, the conductivity of SiMW increases with the introduction of NH_3 gas. Electrons donated from NH_3 act as a chemical gate, cause a band bending, and form an electron accumulation layer due to the molecular gating effect.[67,68] Therefore, the conductivity of the SiMW device increases with the introduction of NH_3 gas.

3.5. Machine Learning-Based Qualification and Quantification. Machine learning techniques were employed to discriminate the gases and predict NH_3 gas concentration. As depicted in Figure 6a, the 2D PCA chart shows that the distribution of the gases appeared to overlap virtually. However, as can be seen in Figure 6b, four distinct groups in the three-dimensional PCA chart of four tested gases can be well discriminated. The total variance of PC1, PC2, and PC3 is 99.42%, indicating a slight loss of information. As the gas concentration increases, the plots for the NH_3 gas tend to orient from left-top to the right-bottom, while the other tested gases are distributed in other directions, from bottom to top and left-bottom to right-top. As demonstrated in Figure 5d, the difference in the response between the NH_3 gas and other gases is significant.

Despite improving visualization, dimension reduction approaches such as PCA are not classified as effective classification techniques.[69] Among the supervised machine learning-based classifier algorithms such as Bayesian network, *k*-nearest neighbor, and RF, the RF algorithm was supposed to be a multi-advantage and high-accuracy prediction algorithm integrated with a single sensor.[70,71] This study implemented RF algorithms to classify gases and concentration prediction. The normalized confusion matrix in Figure 6c shows the correlation between the prediction and the actual labels. The Si VMWA-based gas sensor does not confuse NH_3 gas with the other gases, which illustrates the great distinction of NH_3 gas via the PCA and RF Classifier with a high classification accuracy of 95.95%, further proving the ability to discriminate NH_3 gas against other analytes. The adsorption and desorption processes of gases on the sensing materials are strongly related to the chemical/physical properties of gases.[32] Extracting the relationship between the sensor response and the adsorption/desorption of the analyte is valuable information for enhancing the discrimination of gases using machine learning algorithms, consequently improving the selectivity feature of the sensor. Figure 6d presents the RF regression result, where the points indicate the predicted concentration versus the actual concentration of the NH_3 gas. Most points are positioned on a diagonal line indicating a perfect prediction. The concentrations in the range of 2−500 ppm were well predicted with a high accuracy of 95.36%. This machine learning-based linear fitting curve enhances the prediction ability compared to the curve merely based on the response indicator (range of 2−200 ppm, Figure 4d). The results promise that the detection and the concentration estimation of NH_3 gas can be autonomously decided without human operation.

4. CONCLUSIONS

A cost-effectively uniform Si VMWA-based gas sensor was prepared by combining conventional lithography technology and the optimized MaCE method. Contact aligner photolithography was employed to form the microsized patterns, followed by the deposition of the Ti/Au layer with optimized deposition conditions, which facilitates the successful fab-

https://doi.org/10.1021/acsaelm.2c01383
ACS Appl. Electron. Mater. 2023, 5, 357−366

rication of Si VMWA with different diameters by the MaCE method processing at room temperature. Our optimized MaCE conditions for microsized patterns perform a stable etching reaction lasting at least 6 h and fabricates a highly uniform structure. By governing the MaCE etching time, Si VMWA with the desired length was fabricated for the NH_3 gas sensing device after introducing the AgNW IDE electrode onto the top surface of Si VMWA. The Si VMWA sensors with different diameters (2−5 μm) were fabricated, and their response to ammonia gas was investigated in both air and nitrogen environments. Samples with smaller diameters exhibit a greater response due to the larger absorption surface area. In the air environment, the Si VMWA shows high efficiency in NH_3 gas sensing at room temperature (4%@2 ppm−122%@500 ppm) with the linear response at a concentration range of 2−200 ppm and a limit of detection of 200 ppb. In addition, in a nitrogen environment, the sensor exhibits an extremely high response to NH_3 (40%@2 ppm−7800%@500 ppm). Furthermore, our single gas sensor platform exhibits remarkable selectivity toward NH_3 gas against the others (nitrogen dioxide, isobutane, and toluene). Data from the response curve of Si VMWA sensors to gases were collected as the input data of machine learning processing analysis. PCA and RF classifier algorithms were employed to successfully discriminate NH3 gas with the others. The gas concentration prediction was carried out with the RF regressor algorithm exhibiting a high accuracy prediction (over 95%) to a wide range of gas concentrations (2−500 ppm). Our results broaden the application of silicon material at the microsize and the integration with machine learning to maximize their potential in monitoring highly diluted gas leakage for use in complicated environments. In the future, the modification/functionalization of the SiMW surface with other noble metals or chemicals will further enhance the sensing performance.

■ ASSOCIATED CONTENT

Supporting Information

The Supporting Information is available free of charge at https://pubs.acs.org/doi/10.1021/acsaelm.2c01383.

Chemical and material; instruments; preparation of Si VMWA substrate; fabrication of Si VMWA discussion; SEM images of MaCE etching Si VMWA; response of bulk silicon and AgNWs; response time and recovery rate, response slope determination; and gas sensing mechanism (PDF)

■ AUTHOR INFORMATION

Corresponding Author

Jaekyun Kim − *Department of Photonics and Nanoelectronics, Hanyang University, Ansan 15888, Republic of Korea; BK21 FOUR ERICA-ACE Center, Hanyang University, Ansan 15588, Republic of Korea*; Email: jaekyunkim@hanyang.ac.kr

Authors

Quang Trung Le − *Department of Photonics and Nanoelectronics, Hanyang University, Ansan 15888, Republic of Korea; BK21 FOUR ERICA-ACE Center, Hanyang University, Ansan 15588, Republic of Korea*; orcid.org/0000-0002-2032-3523

Ali Sehpar Shikoh − *Department of Photonics and Nanoelectronics, Hanyang University, Ansan 15888, Republic of Korea; BK21 FOUR ERICA-ACE Center, Hanyang University, Ansan 15588, Republic of Korea*

Kumin Kang − *Department of Photonics and Nanoelectronics, Hanyang University, Ansan 15888, Republic of Korea; BK21 FOUR ERICA-ACE Center, Hanyang University, Ansan 15588, Republic of Korea*

Jeongho Lee − *Department of Photonics and Nanoelectronics, Hanyang University, Ansan 15888, Republic of Korea; BK21 FOUR ERICA-ACE Center, Hanyang University, Ansan 15588, Republic of Korea*; orcid.org/0000-0002-6704-250X

Complete contact information is available at: https://pubs.acs.org/10.1021/acsaelm.2c01383

Author Contributions

Q.T.L. and A.S.S contributed equally. The manuscript was written through contributions of all authors. All authors have given approval to the final version of the manuscript.

Notes

The authors declare no competing financial interest.

■ ACKNOWLEDGMENTS

This work was supported by the research fund of Hanyang University (HY-2021) and National Research Foundation of Korea (NRF) grant funded by the Korea government (MSIT) (no. 2020R1A2C1008968). OM and SEM measurements were carried out with Olympus BX51M and Hitachi S-4700 FE-SEM systems, respectively, at the Hanyang University ERICA Next-Generation Display Research Core Facility.

■ ABBREVIATIONS

MaCE, metal-assisted chemical etching; SiMW, silicon microwire; Si VMWA, silicon vertical microwire arrays; NH_3, ammonia; IDE, interdigitated electrode; PCA, principal component analysis; VOC, volatile organic compounds; MEMS, microelectromechanical systems

■ REFERENCES

(1) Ricci, P. P.; Gregory, O. J. Sensors for the detection of ammonia as a potential biomarker for health screening. *Sci. Rep.* **2021**, *11*, 7185.

(2) Das, S.; Pal, M. Review-Non-Invasive Monitoring of Human Health by Exhaled Breath Analysis: A Comprehensive Review. *J. Electrochem. Soc.* **2020**, *167*, 037562.

(3) Gębicki, J.; Kloskowski, A.; Chrzanowski, W.; Stepnowski, P.; Namiesnik, J. Application of Ionic Liquids in Amperometric Gas Sensors. *Crit. Rev. Anal. Chem.* **2016**, *46*, 122−138.

(4) Kim, H.-J.; Lee, J.-H. Highly sensitive and selective gas sensors using p-type oxide semiconductors: Overview. *Sens. Actuators, B* **2014**, *192*, 607−627.

(5) Hodgkinson, J.; Tatam, R. P. Optical gas sensing: a review. *Meas. Sci. Technol.* **2013**, *24*, 012004.

(6) Ghule, B. G.; Shaikh, S.; Ekar, S. U.; Nakate, U. T.; Gunturu, K. C.; Shinde, N. M.; Naushad, M.; Kim, K. H.; O'Dwyer, C.; Mane, R. S. Natural Carbonized Sugar as a Low-Temperature Ammonia Sensor Material: Experimental, Theoretical, and Computational Studies. *ACS Appl. Mater. Interfaces* **2017**, *9*, 43051−43060.

(7) Bedi, R. K.; Singh, I. Room-Temperature Ammonia Sensor Based on Cationic Surfactant-Assisted Nanocrystalline CuO. *ACS Appl. Mater. Interfaces* **2010**, *2*, 1361−1368.

(8) Lupan, O.; Postica, V.; Marx, J.; Mecklenburg, M.; Mishra, Y. K.; Schulte, K.; Fiedler, B.; Adelung, R. Individual hollow and mesoporous aero-graphitic microtube based devices for gas sensing applications. *Appl. Phys. Lett.* **2017**, *110*, 263109.

(9) Joshi, N.; Braunger, M. L.; Shimizu, F. M.; Riul, A., Jr.; Oliveira, O. N. Insights into nano-heterostructured materials for gas sensing: a review. *Multifunct. Mater.* **2021**, *4*, 032002.
(10) Kwak, D.; Lei, Y.; Maric, R. Ammonia gas sensors: A comprehensive review. *Talanta* **2019**, *204*, 713−730.
(11) Zhang, J.; Liu, L.; Yang, Y.; Huang, Q.; Li, D.; Zeng, D. A review on two-dimensional materials for chemiresistive- and FET-type gas sensors. *Phys. Chem. Chem. Phys.* **2021**, *23*, 15420−15439.
(12) Yu, X. F.; Li, Y. C.; Cheng, J. B.; Liu, Z. B.; Li, Q. Z.; Li, W. Z.; Yang, X.; Xiao, B. Monolayer Ti2CO2: A Promising Candidate for NH3 Sensor or Capturer with High Sensitivity and Selectivity. *ACS Appl. Mater. Interfaces* **2015**, *7*, 13707−13713.
(13) Mackin, C.; Schroeder, V.; Zurutuza, A.; Su, C.; Kong, J.; Swager, T. M.; Palacios, T. Chemiresistive Graphene Sensors for Ammonia Detection. *ACS Appl. Mater. Interfaces* **2018**, *10*, 16169−16176.
(14) Schütt, F.; Postica, V.; Adelung, R.; Lupan, O. Single and Networked ZnO-CNT Hybrid Tetrapods for Selective Room-Temperature High-Performance Ammonia Sensors. *ACS Appl. Mater. Interfaces* **2017**, *9*, 23107−23118.
(15) Sarkar, D.; Xie, X.; Kang, J.; Zhang, H.; Liu, W.; Navarrete, J.; Moskovits, M.; Banerjee, K. Functionalization of transition metal dichalcogenides with metallic nanoparticles: implications for doping and gas-sensing. *Nano Lett.* **2015**, *15*, 2852−2862.
(16) Cao, A.; Sudhölter, E. J.; de Smet, L. C. Silicon Nanowire-Based Devices for Gas-Phase Sensing. *Sensors* **2013**, *14*, 245−271.
(17) Liu, D.; Lin, L.; Chen, Q.; Zhou, H.; Wu, J. Low Power Consumption Gas Sensor Created from Silicon Nanowires/TiO2 Core-Shell Heterojunctions. *ACS Sens.* **2017**, *2*, 1491−1497.
(18) Qin, Y.; Liu, D.; Zhang, T.; Cui, Z. Ultrasensitive Silicon Nanowire Sensor Developed by a Special Ag Modification Process for Rapid NH3 Detection. *ACS Appl. Mater. Interfaces* **2017**, *9*, 28766−28773.
(19) Qin, Y.; Cui, Z.; Zhang, T.; Liu, D. Polypyrrole shell (nanoparticles)-functionalized silicon nanowires array with enhanced NH3-sensing response. *Sens. Actuators, B* **2018**, *258*, 246−254.
(20) Qin, Y.; Zang, J.; Wen, Z. Synergistic functionalization of aligned silicon nanowires by Ag nanoparticles&PPy wrapping for improving gas-sensing response at high humidity level. *Phys. E* **2020**, *118*, 113957.
(21) Um, H.-D.; Lee, K.; Hwang, I.; Park, J.; Choi, D.; Kim, N.; Kim, H.; Seo, K. Progress in silicon microwire solar cells. *J. Mater. Chem. A* **2020**, *8*, 5395−5420.
(22) Huang, Z.; Fang, H.; Zhu, J. Fabrication of Silicon Nanowire Arrays with Controlled Diameter, Length, and Density. *Adv. Mater.* **2007**, *19*, 744−748.
(23) Mallavarapu, A.; Ajay, P.; Sreenivasan, S. V. Enabling Ultrahigh-Aspect-Ratio Silicon Nanowires Using Precise Experiments for Detecting the Onset of Collapse. *Nano Lett.* **2020**, *20*, 7896−7905.
(24) Choi, D.; Seo, K. Field-Induced Radial Junction for Dopant-Free Crystalline Silicon Microwire Solar Cells with an Efficiency of Over 20%. *Adv. Energy Mater.* **2021**, *11*, 2003707.
(25) Yang, Y.; Yuan, W.; Kang, W.; Ye, Y.; Pan, Q.; Zhang, X.; Ke, Y.; Wang, C.; Qiu, Z.; Tang, Y. A review on silicon nanowire-based anodes for next-generation high-performance lithium-ion batteries from a material-based perspective. *Sustainable Energy Fuels* **2020**, *4*, 1577−1594.
(26) Espinosa-Villatoro, E.; Nelson Weker, J.; Ko, J. S.; Quiroga-González, E. Tracking the evolution of processes occurring in silicon anodes in lithium ion batteries by 3D visualization of relaxation times. *J. Electroanal. Chem.* **2021**, *892*, 115309.
(27) Wang, B.; Dong, X.-S.; Wang, Z.; Wang, Y.-F.; Hou, Z.-Y. MEMS-Based Ionization Gas Sensors for VOCs with Array of Nanostructured Silicon Needles. *ACS Sens.* **2020**, *5*, 994−1001.
(28) Zhu, W.; Xu, T.; Liu, W.; Wang, W.; Feng, M.; Cheng, Y.; Li, Y.; Tian, Y.; Li, X. High-performance ethanol sensor based on In2O3 nanospheres grown on silicon nanoporous pillar array. *Sens. Actuators, B* **2020**, *324*, 128734.
(29) Liu, J.; Liang, Y.; Yi, F.; Wang, B.; Zhang, T.; Wang, Y.; Zhou, Y. Gas sensor based on ZnO film/silica pillars. *Mater. Res. Express* **2016**, *3*, 125701.
(30) Akbari-Saatlu, M.; Procek, M.; Mattsson, C.; Thungström, G.; Nilsson, H.-E.; Xiong, W.; Xu, B.; Li, Y.; Radamson, H. H. Silicon Nanowires for Gas Sensing: A Review. *Nanomaterials* **2020**, *10*, 2215.
(31) Fahad, H. M.; Shiraki, H.; Amani, M.; Zhang, C.; Hebbar, V. S.; Gao, W.; Ota, H.; Hettick, M.; Kiriya, D.; Chen, Y. Z.; Chueh, Y. L.; Javey, A. Room temperature multiplexed gas sensing using chemical-sensitive 3.5-nm-thin silicon transistors. *Sci. Adv.* **2017**, *3*, No. e1602557.
(32) Nallon, E. C.; Schnee, V. P.; Bright, C. J.; Polcha, M. P.; Li, Q. Discrimination Enhancement with Transient Feature Analysis of a Graphene Chemical Sensor. *Anal. Chem.* **2016**, *88*, 1401−1406.
(33) Jeong, S. Y.; Jeong, S.; Lee, S. W.; Kim, S. T.; Kim, D.; Jeong, H. J.; Han, J. T.; Baeg, K. J.; Yang, S.; Jeong, M. S.; Lee, G. W. Enhanced response and sensitivity of self-corrugated graphene sensors with anisotropic charge distribution. *Sci. Rep.* **2015**, *5*, 11216.
(34) Bae, G.; Song, D. S.; Lim, Y. R.; Jeon, I. S.; Jang, M.; Yoon, Y.; Jeon, C.; Song, W.; Myung, S.; Lee, S. S.; Park, C. Y.; An, K. S. Chemical Patterning of Graphene via Metal-Assisted Highly Energetic Electron Irradiation for Graphene Homojunction-Based Gas Sensors. *ACS Appl. Mater. Interfaces* **2020**, *12*, 47802−47810.
(35) Tang, H.; Li, Y.; Sokolovskij, R.; Sacco, L.; Zheng, H.; Ye, H.; Yu, H.; Fan, X.; Tian, H.; Ren, T. L.; Zhang, G. Ultra-High Sensitive NO2 Gas Sensor Based on Tunable Polarity Transport in CVD-WS2/IGZO p-N Heterojunction. *ACS Appl. Mater. Interfaces* **2019**, *11*, 40850−40859.
(36) Pedregosa, F.; Varoquaux, G.; Gramfort, A.; Michel, V.; Thirion, B.; Grisel, O.; Blondel, M.; Prettenhofer, P.; Weiss, R.; Dubourg, V.; Vanderplas, J.; Passos, A.; Cournapeau, D.; Brucher, M.; Perrot, M.; Duchesnay, E. Scikit-learn: Machine Learning in Python. *J. Mach. Learn. Res.* **2011**, *12*, 2825−2830.
(37) Van Rossum, G.; Drake, L. F.*Python 3 Reference Manual*; CreateSpace, 2009.
(38) Baek, J.; Jang, B.; Kim, M. H.; Kim, W.; Kim, J.; Rim, H. J.; Shin, S.; Lee, T.; Cho, S.; Lee, W. High-performance hydrogen sensing properties and sensing mechanism in Pd-coated p-type Si nanowire arrays. *Sens. Actuators, B* **2018**, *256*, 465−471.
(39) Oh, M.; Jin, W. Y.; Jeong, H. J.; Jeong, M. S.; Kang, J. W.; Kim, H. Silver Nanowire Transparent Conductive Electrodes for High-Efficiency III-Nitride Light-Emitting Diodes. *Sci. Rep.* **2015**, *5*, 13483.
(40) Lee, S.; Jang, J.; Park, T.; Park, Y. M.; Park, J. S.; Kim, Y. K.; Lee, H. K.; Jeon, E. C.; Lee, D. K.; Ahn, B.; Chung, C. H. Electrodeposited Silver Nanowire Transparent Conducting Electrodes for Thin-Film Solar Cells. *ACS Appl. Mater. Interfaces* **2020**, *12*, 6169−6175.
(41) Murray, B. J.; Walter, E. C.; Penner, R. M. Amine Vapor Sensing with Silver Mesowires. *Nano Lett.* **2004**, *4*, 665−670.
(42) Jain, M. K.*Diluted Magnetic Semiconductors*; World Scientific, 1991.
(43) Lê, Q. T.; Ly, N. H.; Kim, M. K.; Lim, S. H.; Son, S. J.; Zoh, K. D.; Joo, S. W. Nanostructured Raman substrates for the sensitive detection of submicrometer-sized plastic pollutants in water. *J. Hazard. Mater.* **2021**, *402*, 123499.
(44) Urso, M.; Leonardi, S. G.; Neri, G.; Petralia, S.; Conoci, S.; Priolo, F.; Mirabella, S. Room temperature detection and modelling of sub-ppm NO2 by low-cost nanoporous NiO film. *Sens. Actuators, B* **2020**, *305*, 127481.
(45) Yuan, Z.; Bariya, M.; Fahad, H. M.; Wu, J.; Han, R.; Gupta, N.; Javey, A. Trace-Level, Multi-Gas Detection for Food Quality Assessment Based on Decorated Silicon Transistor Arrays. *Adv. Mater.* **2020**, *32*, 1908385.
(46) Sik Choi, M.; Young Kim, M.; Mirzaei, A.; Kim, H.-S.; Kim, S.-i.; Baek, S.-H.; Won Chun, D.; Jin, C.; Hyoung Lee, K. Selective, sensitive, and stable NO2 gas sensor based on porous ZnO nanosheets. *Appl. Surf. Sci.* **2021**, *568*, 150910.
(47) Asgari, M.; Saboor, F. H.; Amouzesh, S. P.; Coull, M. W.; Khodadadi, A. A.; Mortazavi, Y.; Hyodo, T.; Shimizu, Y. Facile

ultrasonic-assisted synthesis of SiO2/ZnO core/shell nanostructures: A selective ethanol sensor at low temperatures with enhanced recovery. *Sens. Actuators, B* **2022**, *368*, 132187.
(48) Xu, P.; Song, K.; Xia, X.; Chen, Y.; Wang, Q.; Wei, G.Temperature and Humidity Compensation for MOS Gas Sensor Based on Random Forests. In *Intelligent Computing, Networked Control, and Their Engineering Applications*; Yue, D., Peng, C., Du, D., Zhang, T., Zheng, M., Han, Q., Eds.; Springer Singapore: Singapore, 2017; pp 135−145.
(49) Pyke, S. C.; Boos, D. L.; Brouwer, M. L.Temperature and humidity compensation for gas detection apparatus. U.S. Patent 4,730,479 A, 1986.
(50) Alford, J. M.; Laaksonen, R. T.; Smalley, R. E. Ammonia chemisorption studies on silicon cluster ions. *J. Chem. Phys.* **1991**, *94*, 2618−2630.
(51) Yang, L.; Lin, H.; Zhang, Z.; Cheng, L.; Ye, S.; Shao, M. Gas sensing of tellurium-modified silicon nanowires to ammonia and propylamine. *Sens. Actuators, B* **2013**, *177*, 260−264.
(52) Wang, J.; Li, Z.; Zhang, S.; Yan, S.; Cao, B.; Wang, Z.; Fu, Y. Enhanced NH3 gas-sensing performance of silica modified CeO2 nanostructure based sensors. *Sens. Actuators, B* **2018**, *255*, 862−870.
(53) Mhlongo, G. H.; Motaung, D. E.; Swart, H. C. Pd2+ doped ZnO nanostructures: Structural, luminescence and gas sensing properties. *Mater. Lett.* **2015**, *160*, 200−205.
(54) Panes-Ruiz, L. A.; Shaygan, M.; Fu, Y.; Liu, Y.; Khavrus, V.; Oswald, S.; Gemming, T.; Baraban, L.; Bezugly, V.; Cuniberti, G. Toward Highly Sensitive and Energy Efficient Ammonia Gas Detection with Modified Single-Walled Carbon Nanotubes at Room Temperature. *ACS Sens.* **2018**, *3*, 79−86.
(55) Wu, M.; He, M.; Hu, Q.; Wu, Q.; Sun, G.; Xie, L.; Zhang, Z.; Zhu, Z.; Zhou, A. Ti3C2 MXene-Based Sensors with High Selectivity for NH3 Detection at Room Temperature. *ACS Sens.* **2019**, *4*, 2763−2770.
(56) Kumar, C.; Rawat, G.; Kumar, H.; Kumar, Y.; Prakash, R.; Jit, S. Electrical and ammonia gas sensing properties of poly (3, 3‴-dialkylquaterthiophene) based organic thin film transistors fabricated by floating-film transfer method. *Org. Electron.* **2017**, *48*, 53−60.
(57) Tu, Y.; Kyle, C.; Luo, H.; Zhang, D. W.; Das, A.; Briscoe, J.; Dunn, S.; Titirici, M. M.; Krause, S. Ammonia Gas Sensor Response of a Vertical Zinc Oxide Nanorod-Gold Junction Diode at Room Temperature. *ACS Sens.* **2020**, *5*, 3568−3575.
(58) Chang, S. J.; Weng, W. Y.; Hsu, C. L.; Hsueh, T. J. High sensitivity of a ZnO nanowire-based ammonia gas sensor with Pt nano-particles. *Nano Commun. Netw* **2010**, *1*, 283−288.
(59) Sharma, S.; Kumar, A.; Singh, N.; Kaur, D. Excellent room temperature ammonia gas sensing properties of n-MoS2/p-CuO heterojunction nanoworms. *Sens. Actuators, B* **2018**, *275*, 499−507.
(60) Qiang, X.; Hu, M.; Zhao, B.; Qin, Y.; Zhang, T.; Zhou, L.; Liang, J. Preparation of porous silicon/Pd-loaded WO 3 nanowires for enhancement of ammonia sensing properties at room temperature. *Mater. Sci. Semicond. Process.* **2018**, *79*, 113−118.
(61) Fujisawa, M.; Taguchi, Y.; Kuwahara, Y.; Onchi, M.; Nishijima, M. Electron-energy-loss spectra of the Si(100)-(2×1) surface exposed toNH3. *Phys. Rev. B: Condens. Matter Mater. Phys.* **1989**, *39*, 12918−12920.
(62) Dresser, M. J.; Taylor, P. A.; Wallace, R. M.; Choyke, W. J.; Yates, J. T. The adsorption and decomposition of NH3 ON Si(100)-detection of the NH2(a) species. *Surf. Sci.* **1989**, *218*, 75−107.
(63) Widjaja, Y.; Mysinger, M. M.; Musgrave, C. B. Ab Initio Study of Adsorption and Decomposition of NH3 on Si(100)-(2×1). *J. Phys. Chem. B* **2000**, *104*, 2527−2533.
(64) Wang, W.; Xu, X. Mechanisms for NH3 Decomposition on the Si(111)-7 × 7 Surface: A DFT Cluster Model Study. *J. Phys. Chem. C* **2007**, *111*, 16974−16981.
(65) Neergaard Waltenburg, H.; Yates, J. T. Surface Chemistry of Silicon. *Chem. Rev.* **1995**, *95*, 1589−1673.
(66) Li, C.; Krali, E.; Fobelets, K.; Cheng, B.; Wang, Q. Conductance modulation of Si nanowire arrays. *Appl. Phys. Lett.* **2012**, *101*, 222101.
(67) Kong, J.; Franklin, N. R.; Zhou, C.; Chapline, M. G.; Peng, S.; Cho, K.; Dai, H. Nanotube Molecular Wires as Chemical Sensors. *Science* **2000**, *287*, 622−625.
(68) Kim, D.; Park, C.; Choi, W.; Shin, S.-H.; Jin, B.; Baek, R.-H.; Lee, J.-S. Improved Long-Term Responses of Au-Decorated Si Nanowire FET Sensor for NH3 Detection. *IEEE Sens. J.* **2020**, *20*, 2270−2277.
(69) Cheriyadat, A.; Bruce, L. M.Why principal component analysis is not an appropriate feature extraction method for hyperspectral data. *2003 IEEE International Geoscience and Remote Sensing Symposium (IEEE Cat. no. 03CH37477)*, 21−25 July 2003, 2003; Vol. *3426*, pp 3420−3422.
(70) Kanaparthi, S.; Singh, S. G. Discrimination of gases with a single chemiresistive multi-gas sensor using temperature sweeping and machine learning. *Sens. Actuators, B* **2021**, *348*, 130725.
(71) Acharyya, S.; Jana, B.; Nag, S.; Saha, G.; Guha, P. K. Single resistive sensor for selective detection of multiple VOCs employing SnO2 hollowspheres and machine learning algorithm: A proof of concept. *Sens. Actuators, B* **2020**, *321*, 128484.

https://doi.org/10.1021/acsaelm.2c01383
ACS Appl. Electron. Mater. 2023, 5, 357−366